THE ASTROPHYSICAL JOURNAL, 540:224–235, 2000 September 1

BIPOLAR HYPERSHELL GALACTIC CENTER STARBURST MODEL: FURTHER EVIDENCE FROM *ROSAT* DATA AND NEW RADIO AND X-RAY SIMULATIONS

YOSHIAKI SOFUE
Institute of Astronomy, University of Tokyo, Mitaka, Tokyo 181-8588; sofue@ioa.s.u-tokyo.ac.jp
Received 1999 September 6; accepted 2000 January 20

ABSTRACT

Using the all-sky *ROSAT* soft X-ray and 408 MHz radio continuum data, we show that the North Polar Spur (NPS) and its western and southern counterspurs draw a giant dumbbell shape necked at the Galactic plane. We interpret these features as due to a shock front originating from a starburst 15 million years ago with a total energy of the order of $\sim 10^{56}$ ergs or 10^5 Type II supernovae. We simulate all-sky distributions of radio continuum and soft X-ray intensities based on the bipolar hypershell Galactic center starburst model. The simulations can well reproduce the radio NPS and related spurs, as well as radio spurs in the tangential directions of spiral arms. Simulated X-ray maps in the 0.25, 0.75, and 1.5 keV bands reproduce the *ROSAT* X-ray NPS, its western and southern counterspurs, and the absorption layer along the Galactic plane. We propose to use the *ROSAT* all-sky maps to probe the physics of gas in the halo-intergalactic interface, and to directly date and measure the energy of a recent Galactic center starburst.

Subject headings: galaxies: starburst — Galaxy: center — radio continuum: general — X-rays: general

1. INTRODUCTION

A bipolar hypershell model has been proposed for the North Polar Spur (NPS) (Sofue 1977), in which the NPS and its western and southern counterspurs are interpreted as due to a dumbbell-shaped shock front induced by a giant explosive event at the Galactic center. Such an impulsive energy input may have been originated by a starburst 15 million years ago (Sofue 1984, 1994). An alternative mechanism for causing such giant shells in the halo would be a single energetic explosion at the Galactic nucleus (Oort 1977). Giant shell structures could also be produced by a stellar wind–driven coherent galactic wind (e.g., Heckman, Armus, & Miley 1990). Since the cooling time in the halo is much longer than the shell's lifetime, any of these mechanisms will, however, result in similar shocked shells in the halo, given the same amount of total energy. Another alternative, traditional idea to explain the NPS is the local-shell hypothesis, in which the NPS is interpreted as due to a very unique supernova remnant of the largest diameter in the Galaxy (Berkhuijsen, Haslam, & Salter 1971; Egger 1993; Egger & Aschenbach 1995 and literature cited therein).

The propagation of a shock front in the Galactic halo can be simulated by applying a shock-tracing method developed by Sakashita (1971) and Möllenhoff (1976) to a case of point explosion at a center of a disk surrounded by a halo and intergalactic uniform gas (Sofue 1984). The Galactic center explosion hypothesis tries to explain the NPS, as well as the other spurs surrounding the Galactic center region, by a single Galactic event, based not only on the morphology but also on a distance estimate of NPS from soft X-ray extinction (Sofue 1994).

In the present paper, we revisit the Galactic center explosion hypothesis. We will extend the arguments given in Sofue (1994), which were based on the Wisconsin X-ray experiment's data (McCammon et al. 1983; McCammon & Sanders 1990). We will discuss the origin of the NPS and related galactic spurs, using the 408 MHz all-sky radio data (Haslam et al. 1982) and the *ROSAT* X-ray images (Snowden et al. 1997). We simulate X-ray all-sky views based on the bipolar hypershell (BHS) model in order to reproduce morphologically the *ROSAT* all-sky views at various energy bands. We also discuss the implication of the bipolar hypershell in dating and measuring the recent Galactic starburst. We further propose to use the *ROSAT* all-sky data to probe the physics of gas in the Galactic halo and intergalactic space of the Local Group.

2. ALL-SKY RADIO AND X-RAY DATA

2.1. *All-Sky Views*

In Figure 1 we compare the radio and X-ray views of the whole sky in the (l, b) coordinates in Aitoff diagrams. Figure 1*a* shows an enhanced view of Galactic radio spurs obtained by applying a relieving technique (Sofue 1993) to the 408 MHz all-sky map (Haslam et al. 1982). Figure 1*b* is the *ROSAT* all-sky map in the R45 (~ 0.75 keV) band as reproduced from Snowden et al. (1997). These figures demonstrate that the major Galactic spurs in both radio and X-rays are found in the central 100° ($\pm 50°$) region around the Galactic center. The NPS and its western and southern counterparts compose giant Ω shapes, drawing a dumbbell shape centered on the Galactic center and necked at the Galactic plane.

2.2. *Radio Spurs*

Figure 2 shows a radio view in a 100° squared region around the Galactic center. Here, a relieving method to enhance the spurs has been applied in the direction of longitude (*left panel*) and in the radial direction (*right panel*). The NPS comprises a well-defined radio arc anchored to the Galactic plane at $l \sim \pm 20°$ and draws a giant arc toward the north Galactic pole. The radio brightness along the NPS increases toward the Galactic plane, attaining a maximum at (l, b) $\sim$ (20°, 0°). The width of the spur (half-intensity length across) decreases toward the Galactic plane, and, therefore, the NPS ridge becomes sharper toward the Galactic plane (Sofue & Reich 1979).

The NPS draws a giant loop toward high latitudes and returns to the Galactic plane, where it merges with a spur emerging from the Galactic plane at $l \sim 340°$. We call this western spur NPS-West. The western half of Loop IV

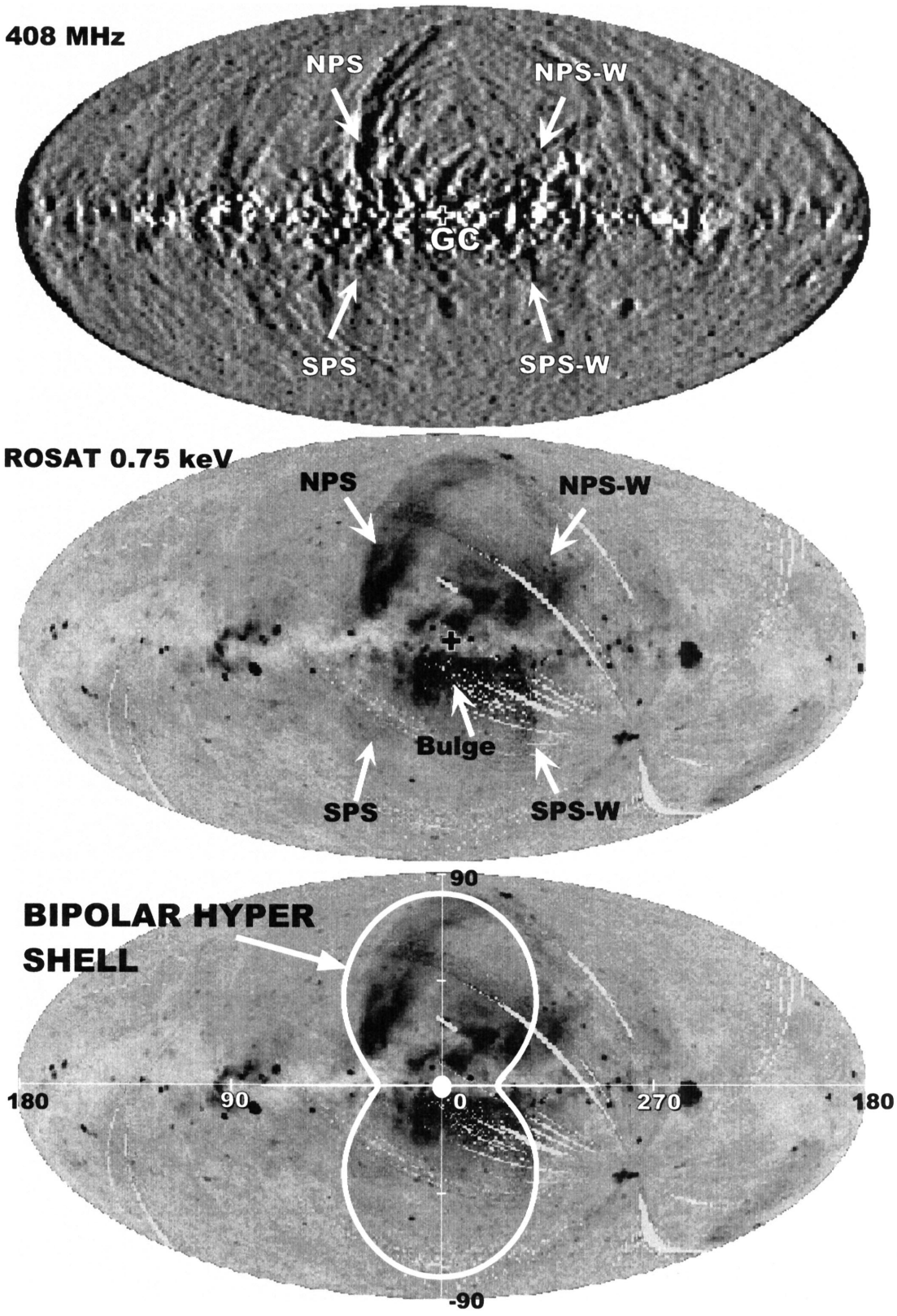

FIG. 1.—*Top*: Enhanced view of galactic spurs in the 408 MHz radio continuum, as obtained by applying a relieving method to the Bonn-Parkes all-sky survey in the Galactic coordinates (Haslam et al. 1982). Major features discussed in the text are indicated by arrows. The Galactic center is at the map center, and the longitude increases toward the left with both side edges being at $l = 180°$. The north Galactic pole is at the top, and the south pole at the bottom. *Middle*: An X-ray all-sky image in the R45 (0.75 keV) band as reproduced from the *ROSAT* survey (Snowden et al. 1997). *Bottom*: Schematic overlay of the BHS on the *ROSAT* 0.75 keV map.

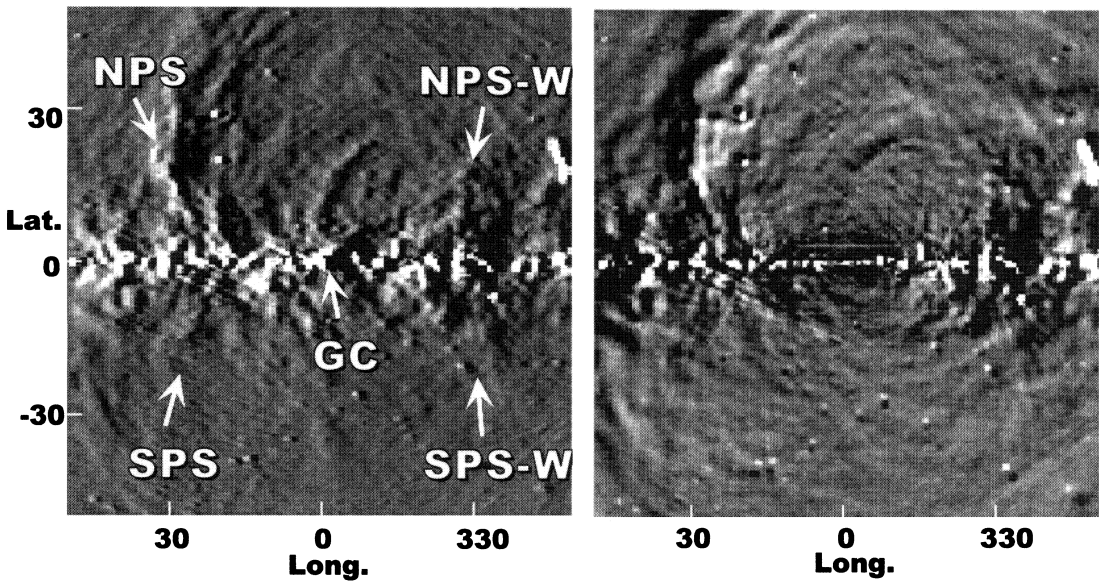

FIG. 2.—408 MHz radio map in a $\pm 50°$ square region around the Galactic center. A relieving method has been applied in the direction of longitude (*left*) and radial direction (*right*). Symmetric sets of spurs emerging from $l \sim 20°$ and $l \sim 340°$ are recognized, which are labeled as NPS, NPS-West, SPS, and SPS-West (see text).

makes a part of NPS-West, and Loop IV itself is highly asymmetric and lacks its eastern half. The NPS and NPS-West, thus, compose a giant Ω shape in the halo above the Galactic center, with its axis roughly coinciding with the Galactic rotation axis at $l = 0°$. A southern counterpart of the NPS, which we call the South Polar Spur (SPS), is visible at $l \sim 20°$, extending from $(l, b) \sim (20°, 0°)$ toward $(30°, -30°)$. Also, a western counterpart of SPS, which we call SPS-West, is found at $(l, b) \sim (340°, 0°)$ to $(320°, -30°)$.

These four spurs, NPS, NPS-West, SPS, and SPS-West, are the most prominent features among the numerous galactic radio spurs. These four spurs compose a huge dumbbell shape necked at the Galactic plane and are about symmetric with respect to the Galactic center. We comment that Loop I, which has been defined as a complete loop of diameter 120° centered on $(l, b) = (330°, 30°)$, is hard to trace in the present enhanced images (Figs. 1 and 2).

2.3. *X-Ray Spurs*

As shown in Figure 1*b*, the R45-band (0.75 keV) X-ray intensity at $b > 10°$ has a global enhancement around the Galactic center, which is due to the high-temperature gas in the Galactic bulge (McCammon et al. 1983). Snowden et al. (1997) have further noticed cylindrical features in the R45 and R67 (1.5 keV) band maps, which emerge from the central Galactic disk toward the halo. They also attribute these features to high-temperature gas around the Galactic center. This fact indicates that the local H I disk is transparent at $b > \sim 10°$ for X-rays at ≥ 0.75 keV.

A giant shell structure of the NPS is clearly visible in the R45 and R67 bands. In Figure 3, we compare the radio and R45-band images of the NPS. The western end of the X-ray NPS also returns to the Galactic plane at $l \sim 340°$ (NPS-West) and draws a giant Ω together with the NPS. Southern

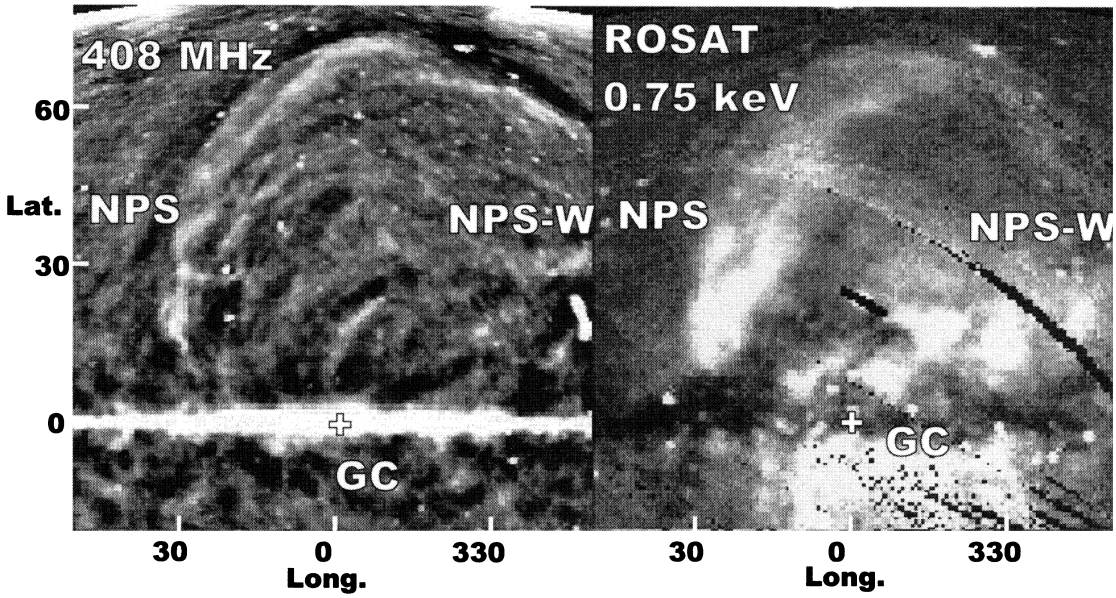

FIG. 3.—Enhanced radio (*left*) and X-ray (*right*) images of the North Polar Spur. Displayed area is $\pm 50°$ square centered at $(l, b) = (0°, 30°)$

counterparts to these features are also visible. Particularly, the SPS-West is clearly recognized in X-rays: an R45-band spur emerges from $l \sim 340°$ toward the southern Galactic pole, which is symmetric to the NPS about the Galactic center. The SPS is also visible at $l \sim +30°$, though fainter in R45 band, while it is more clearly visible in an R45/R67 ratio map. These northern and southern X-ray spurs are associated with the radio spurs (NPS, NPS-West, SPS, and SPS-West) and draw a dumbbell-shape necked at the Galactic plane. We may, hence, reason that the "cylinder" of Snowden et al. (1997) would comprise the NPS, NPS-West, SPS, and SPS-West.

The R12-band (0.25 keV) X-ray emission from the NPS is strongly absorbed below $b = 60°$ and is hardly visible below 30° (Snowden et al. 1997). The NPS shows up most clearly in the R45 band (0.75 keV), while the emission is significantly absorbed in the Galactic disk at $b < 10°$. R67-band (1.5 keV) X-rays are also strongly absorbed near the Galactic plane, indicating that the X-rays from the NPS originate in the space farther than the H I disk (Sofue 1994). Moreover, the X-rays become harder toward the Galactic plane, as indicated by the clear decrease in the R45 to R67 intensity ratio toward the Galactic plane. By comparing the R45- and R12-band intensities, we have shown the H I mass toward $b = 30°$ to be 7×10^{20} H cm^{-2}, which is greater than the observed value (5×10^{20} H cm^{-3}). Sofue (1994) has shown that the X-rays at $b \sim 30°$ originate *beyond* the hydrogen layer, and the distance is greater than 0.6 kpc. Namely, the NPS is an object that is located in the Galactic halo. The distance to the NPS has been subject to debate. We now know that it is beyond 0.6 kpc, which would allow us two possible interpretations. One possibility is that the NPS is a local object at $\sim$1 kpc, originating from supernova explosions at high altitude out of the Galactic plane. Another possibility is that it is a galactic-scale object related to the Galactic center activity.

3. COMPARISON OF BIPOLAR HYPERSHELL MODEL WITH DATA

3.1. *BHS Model*

We interpret the observed radio and X-ray features in terms of the Galactic center explosion hypothesis. Our idea is based on the symmetric appearance of the radio and X-ray shells with respect to the Galactic plane and the Galactic center, which compose a huge dumbbell shape apparently centered on the Galactic center (GC). We assume here that the center of the dumbbell coincides with the GC, and we take the distance to the GC to be 8 kpc. Then the radius of each shell is several kpc. Our idea is also based on the fact that many spiral galaxies exhibit galactic-scale outflows in the forms of dumbbell-shaped shocks, bipolar cylinders, and galactic-scale jets, and we consider that the Milky Way Galaxy would have experienced similar phenomena.

NGC 253 exhibits dumbbell-shaped shells in X-rays above and below the galactic plane, each about 5 kpc in diameter (Vogler & Pietsch 1999a; Pietsch et al. 2000), which would be a result of a starburst and related outflow (Heckmann et al. 1990). NGC 3079 exhibits a pair of radio continuum shells in the halo in both sides of the nucleus, each about 3 kpc in diameter, which is considered to be an ejection from the central activity (Duric et al. 1983). It also exhibits an Hα cone-shaped shell of radius about 1 kpc, coaxial to the radio shells, most likely induced by an outburst from the nuclear region (Veilleux et al. 1994). M82 is a starburst galaxy, which ejects a Galactic-scale flow through bipolar cylindrical jets (Nakai et al. 1987). We emphasize that all these out-of-plane features, including the hypershell in the Milky Way, require a similar amount of total energy input in the central regions of the galaxies, which is of the order of 10^{55}–10^{56} ergs (e.g., Pietsch et al. 2000), or equivalent to 10^4–10^5 Type II supernovae.

3.2. *Adiabatic Shock Envelope Method*

The propagation of a shock wave through the Galactic halo induced by a point energy injection at the Galactic center can be calculated by applying the shock envelope–tracing method of Sakashita (1971) and Möllenhoff (1976). They have extended the Laumbach and Probstein method for tracing the evolution of a shock front to a case of axisymmetric distributions of ambient gas (Laumbach & Probstein1969). The flow field is assumed to be locally radial, and the gas is adiabatic, and, therefore, the heat transfer by radiation and counterpressure are neglected. The density contrast between the shock front and ambient gas is given by $(\gamma + 1)/(\gamma - 1) = 4$ for $\gamma = 5/3$, where γ is the adiabatic exponent of the gas. For a typical density of 10^{-3} H cm^{-3} and temperature of 10^7 K for the shock-heated halo gas, the cooling time due to the free-free thermal emission is approximately 5×10^8 yr. Hence, the assumption of adiabatic gas is valid in our calculation, in which the shell's lifetime is estimated to be of the order of 10^7 yr, as shown below.

The equation of motion of the shock wave is given by (Möllenhoff 1976):

$$E = \int_0^R \frac{P}{\gamma - 1} 4\pi r^2 dr + \int_0^R \frac{1}{2} \left(\frac{\partial r}{\partial t}\right)^2 \rho_0 4\pi r_0^2 dr_0 .$$

Here, E is the total energy of the explosion, P is the internal pressure, γ is the adiabatic exponent, which is assumed to be 5/3 hereafter, ρ_0 is the unperturbed ambient gas density, r is the radius from the explosion center, with suffix 0 denoting the quantities of the unperturbed ambient gas, and R is the radius of the shock front. Assuming that the snowplowed mass is strongly concentrated near the front, the above equation leads to an equation to express the shock radius R as follows (Sakashita 1971; Möllenhoff 1976):

$$E = \frac{1}{3(\gamma + 1)^2} \left(\frac{4(2\gamma - 1)}{(\gamma - 1)} JR\ddot{R} + \left\{ \left[2IR + \frac{8\gamma}{(\gamma + 1)} + 3 \right] J + \frac{2M(\gamma + 1)}{(\gamma - 1)} \right\} \dot{R}^2 \right) .$$

Here,

$$I = \left(\frac{4\pi}{r_0} \frac{d\rho_0}{dr_0} \right)_R ,$$

$$J = \int_0^R \rho_0 4\pi r_0^2 dr_0 ,$$

and

$$M = \rho_0 \frac{4\pi}{3} R^3 .$$

The unperturbed density distribution of gas is assumed to comprise a stratified disk, a halo with an exponentially decreasing density, and intergalactic gas with uniform density. The hydrogen density in the Galactic plane is taken to be 1 H cm^{-3} in the solar vicinity. The gas distribution is approximated by the following expression:

$$\rho_0 = \rho_1 \exp(-z/z_1) + \rho_2 \exp(-z/z_2) + \rho_3 .$$

Here, suffices 1, 2, and 3 denote quantities for the disk, halo, and intergalactic gas, respectively, ρ is the density, z is the height from the Galactic plane, z_i is the scale thickness of the disk and halo. Here, ρ_1, ρ_2, and ρ_3 are ~ 1, 0.01, and 10^{-5} H cm^{-1}, and z_1 and z_2 are ~ 0.1 and 1 kpc, respectively.

This model has been applied to the Galactic center in order to fit the North Polar Spur (Sofue 1984, 1994). The dumbbell-shaped shell structure and the NPS are well reproduced by a case in which the explosion energy is $E = 3 \times 10^{56}$ ergs. Figure 4 shows a calculated shock front at $t = 10$ and 20 Myr as reproduced from Sofue (1984). In this model, the expansion velocity of the shock front amounts to several hundred km s^{-1} and the gas is heated up to 10^7 K, emitting soft X-rays observable in the *ROSAT* energy bands at ~ 0.25, 0.75, and 1.5 keV.

Numerical simulations of smaller scale outflows from the Galactic plane have been obtained in hydrodynamic scheme (e.g., Tomisaka & Ikeuchi 1988) and in MHD (magnetohydrodynamic) treatment (e.g., Uchida, Shibata, & Sofue 1985). However, these simulations have been obtained only for smaller scale outflows with scales less than 1 kpc, so they cannot be applied to the present case with much larger scale shells expanding from the upper halo to the intergalactic space.

3.3. *Radio and X-Ray Simulations*

3.3.1. *Radio Sky*

We simulate radio and X-ray intensity distributions on the sky based on the bipolar hypershell model. In order to simulate the radio and X-ray emissivity in the bipolar hypershells, as calculated above, we approximate the shape of each half of the dumbbell-shaped shock by an ellipse. Here, we calculate a case for a shell whose center is at $z = \pm 6$ kpc and whose radii are 6 and 9 kpc in the radial and vertical (z) directions, respectively. The volume emissivity of synchrotron radiation is calculated from the density contrast of the shocked gas, in which magnetic fields and cosmic-ray electrons are considered to be compressed adiabatically with shock compression of the halo gas, and the volume emissivity of synchrotron radio radiation is assumed to be proportional to $(\rho/\rho_0)^\beta$, with β being approximately 4, where ρ and ρ_0 are gas densities in the shocked shell and unperturbed halo gas, respectively. In the present simulation, the profile of radio emissivity perpendicular to the shell surface is simply represented by an exponentially decreasing function behind the shock front toward the center with a scale thickness of 500 pc (Fig. 4). The emissivity also decreases with the height from the Galactic plane with a scale height of 3 kpc, corresponding to exponentially decreasing density of the halo gas.

In addition to the hypershell, we assume the existence of a Galactic disk of scale height of 0.5 kpc and scale radius of 6 kpc, which is further embedded in a fatter disk with 3 and 8 kpc scale height and radius, respectively. The emissivity is,

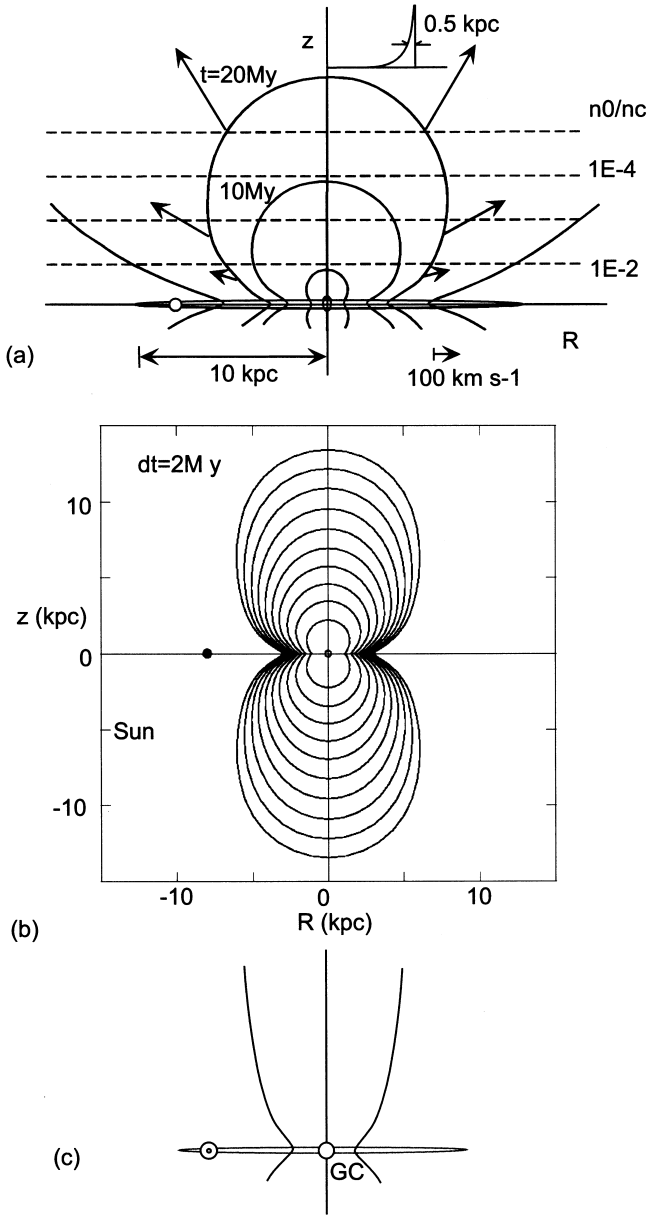

FIG. 4.—(*a*) Calculated shock front in the Galactic halo at 1 and 2×10^7 yr after an explosion and/or a starburst at the nucleus with a total energy of 3×10^{56} ergs (Sofue 1984). (*b*) Same as (*a*), but showing the shock front every 2 Myr. (*c*) Schematic view of a bipolar conical shock front for a case of lower gas density in the upper halo and intergalactic space.

therefore, assumed to have the form expressed by

$$\epsilon = \epsilon_s + \epsilon_1 + \epsilon_2 = \epsilon_s + \epsilon_0 \Sigma_{i=1}^{2} \exp(-r/r_i - z/z_i) ,$$

where ϵ_s is the emissivity in the shell as described above (Fig. 4), ϵ_0 is a constant, ϵ_1 and ϵ_2 represent the disk and fat components, respectively, $r_1 = 6$ kpc, $z_1 = 0.5$ kpc, $r_2 = 8$ kpc, and $z_2 = 3$ kpc. No extinction in the radio band is assumed throughout the Galactic disk and halo. In Figure 5*a* we show the radio continuum result and compare with the observed 408 MHz all-sky map (Fig. 5*c*). The global radio distribution is well reproduced by the model, and the NPS is reproduced as a radio ridge emanating from the Galactic disk.

3.3.2. *Radio Sky with Spiral Arms*

We further simulate a case in which the disk component comprises logarithmic spiral arms, as illustrated in Figure 6.

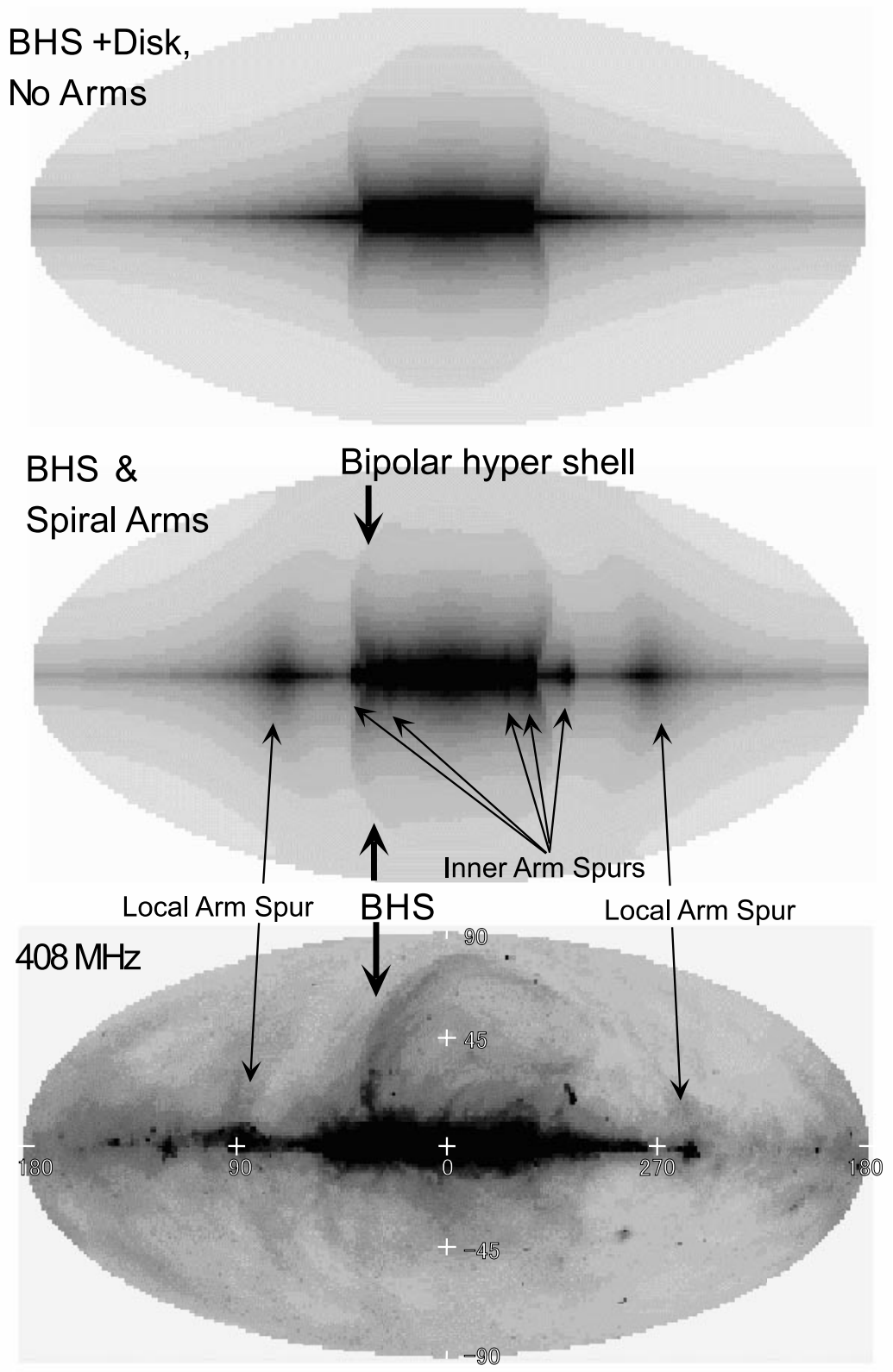

FIG. 5.— Simulated all-sky radio intensity distribution in the galactic coordinates according to the bipolar hypershell model. Intensity scales are relative, and absolute values are arbitrary. (*a*) Hypershells with a flat Galactic disk and a thick disk without spiral arms. (*b*) Hypershells with a Galactic disk comprising logarithmic spiral arms and a thick disk. (*c*) Observed 408 MHz all-sky map in gray scale (Haslam et al. 1982). Thick arrows indicate the bipolar hypershell. Thin arrows indicate the tangential directions of the local and inner spiral arms, where radio spurs are emerging from the disk toward the halo.

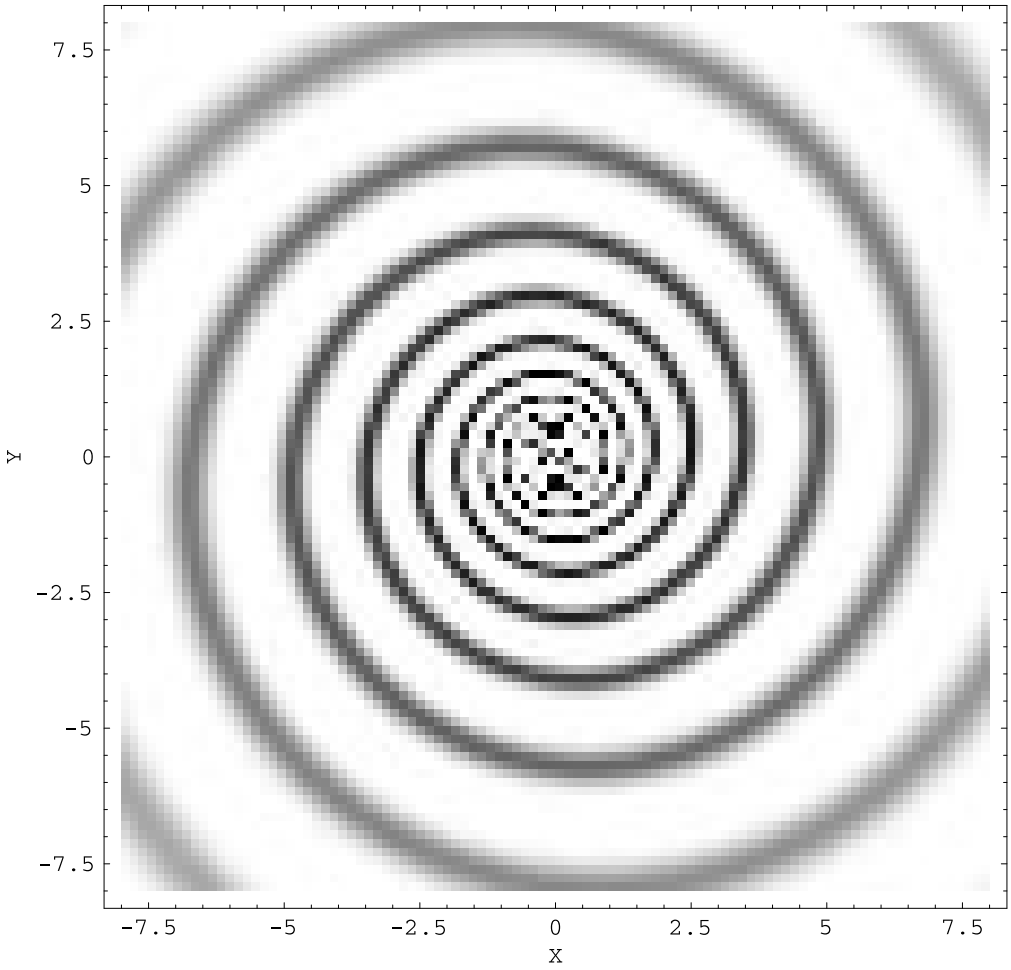

FIG. 6.—Logarithmic spiral arms with pitch angle of 6° and condensation of about 5 times the averaged value

The radio continuum emissivity is assumed to have a form

$$\epsilon_1 = \alpha\epsilon_0 \exp(-r/r_1 - z/z_1) \cos^k(\theta - \eta \log r/r_0) .$$

Here, θ is the Galactocentric azimuthal angle, η is the inverse of the pitch angle of spiral arms, $\eta = 1/\tan p$ with $p = 6°$, $\alpha = 5.1$ is a correction factor to fix the total luminosity to be the same as that when no spiral arms are assumed, and $k = 16$ is introduced to mimic a narrow condensation of the emissivity in the arms. The simulated result is shown in Figure 5*b*. In addition to the spurs due to the hypershells as in Figure 5*a*, there appear many spurs extending toward high latitudes in both sides of the Galactic plane. These spurs are tangential views of bank-shaped spiral arms, which are extending into the halo. It is interesting to note that the tangential directions of the local spiral arms coincide with the western halves of Loop I, Loop II, and Loop III, which was already pointed out earlier (Sofue 1976). Simulated inner-arm spurs are also found to reproduce many observed inner radio spurs, while their exact positional coincidence is out of the present simplified spiral arm model.

3.3.3. *X-Ray Sky*

X-ray emission from the hypershells is assumed to be thermal free-free radiation, whose emissivity is given by

$$\epsilon = n_e^2 \Lambda \propto \rho^2 T^{1/2} .$$

Here, Λ is the cooling function of the gas. Since the temperature is as high as $T \sim 10^7$ K in our simulation, the radiation is almost totally free-free, and the contribution by recombination lines from hydrogen, helium, and metals, which are significant at $T \sim 10^4$–10^6 K, is not significant. For a typical density and temperature of about 10^{-3} H cm^{-3} and 10^7 K, respectively, the value of Λ is 10^{-21} ergs cm^{-9} s^{-1}, and the emissivity is approximately 10^{-27} ergs cm^{-3} s^{-1}. A typical emission measure along the hypershell ridge is $n_e^2 L \sim 10^{-2}$ cm^{-6} pc for a tangential pass in the shell of about 2 kpc. For simplicity, we assume that the temperature of X-ray emitting gas is constant in the shocked shell. The assumption of constant temperature may not be a good approximation for lower latitude regions, where the propagation velocity is lower than that of the upper part, and, therefore, the temperature is lower. However, the low-latitude regions are strongly absorbed by the H I gas layer, and such temperature gradient in the shell would not much improve the accuracy of the present simulation.

In addition to the hypershells, we assume a galactic ridge X-ray component of scale height of 500 pc and a bulge component of scale radius 1 kpc. Emission from ambient halo gas is neglected, because the temperature and density will not be sufficiently high to emit X-rays in the present energy bands.

The X-ray intensity, I, is calculated by a transfer equation given by

$$dI = \epsilon_X ds - \kappa I ds ,$$

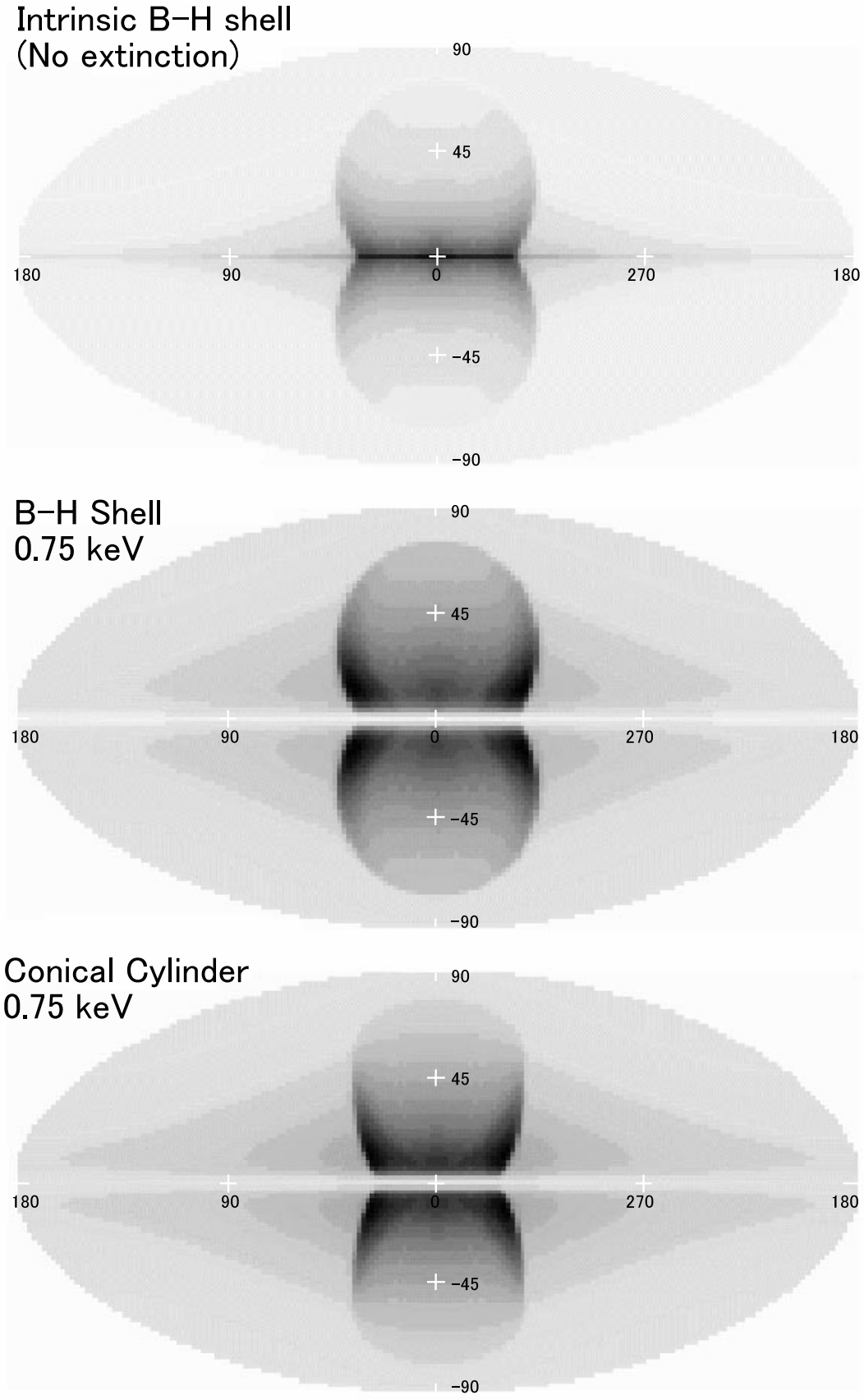

FIG. 7.—Simulated all-sky distributions in the R45 (0.75 keV) X-ray bands. (*a*) Intrinsic intensities of the hypershells and disk without interstellar extinction. (*b*) Intensity distribution for an exponential hydrogen-absorbing layer, but without spiral arms. (*c*) Same as (*b*), but for a parabolic conical cylinder. The Ω shape of the North Polar Spur is better reproduced by the hypershell model of (*b*).

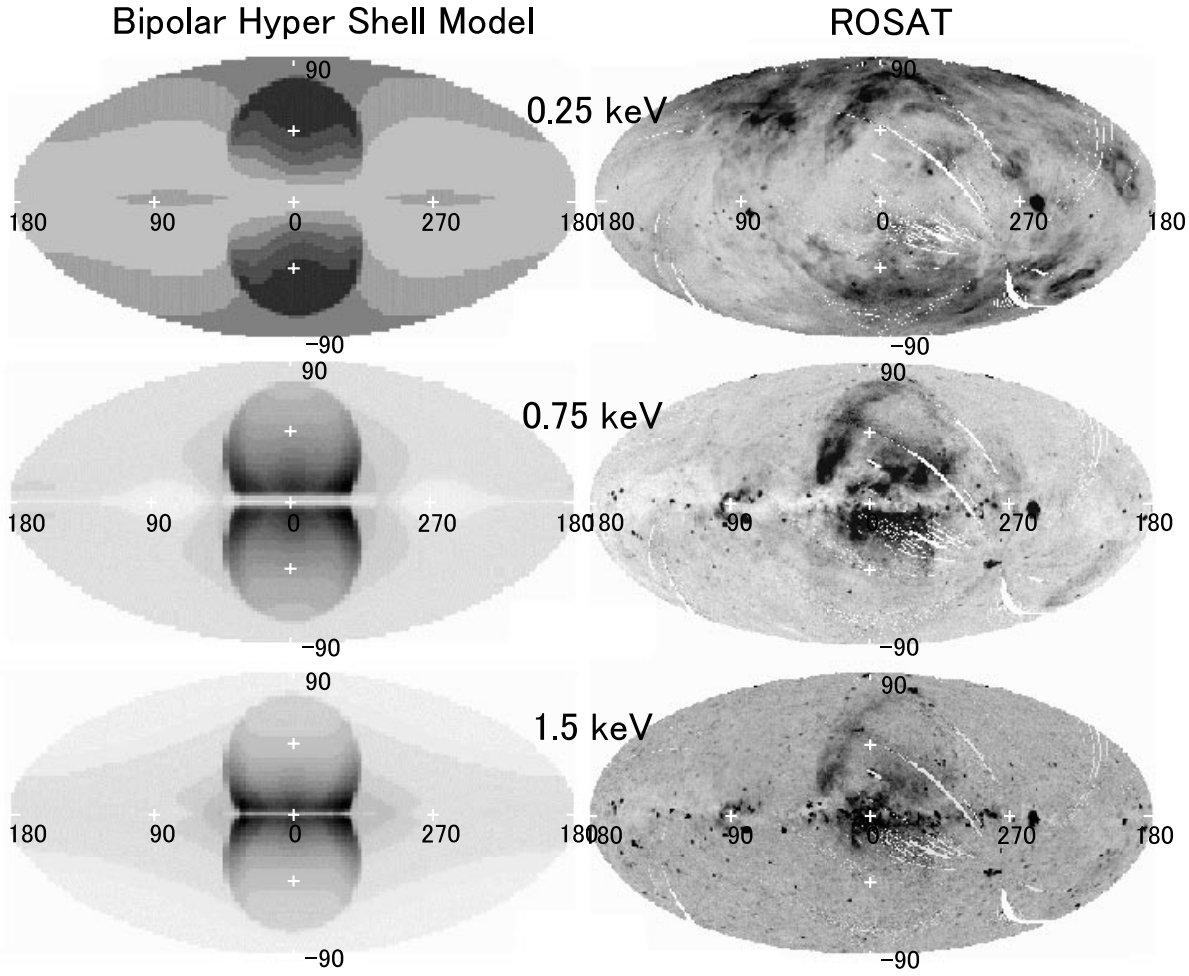

FIG. 8.—Simulated all-sky X-ray views (*left*) compared with the corresponding *ROSAT* sky views (*right*): *top*, R12 (0.25 keV); *middle*, R45 (0.75 keV); *bottom*, R67 (1.5 keV) bands. The absorbing hydrogen layer is assumed to comprise logarithmic spiral arms as in Fig. 6. The polar caps in 0.25 keV band, dumbbell-shaped morphology in 0.75 and 1.5 keV bands, and the absorption features along the Galactic plane are well reproduced by the BHS model calculations.

where the first term on the right-hand side is the emission measure, with ϵ_X being the X-ray emissivity, and the second term represents the absorption rate, with κ being the absorption coefficient and s being the distance along the line-of-sight.

The interstellar extinction of soft X-rays occurs because of photoelectric absorption by metals and has been calculated for the solar metal abundance by Morrison & McCammon (1983). The energy dependence of the cross section per H atoms can be approximated by $\sigma \propto E^{-2.5}$ (Ryter 1996) in the present energy bands, where E is the photon energy of X-rays. The absorption coefficient κ is, then, approximately represented by

$$\kappa = (n_H/N_H^0)(E/E_0)^{-2.5} ,$$

where n_H is the number density of hydrogen atoms and N_H^0 is the e-folding column density of interstellar neutral hydrogen at the photon energy E_0. At $E_0 = 0.75$ keV, the cross section is $\sigma = 4 \times 10^{-22}$ cm^2 per H atom, which yields an e-folding column density of 2.5×10^{21} H atoms. According to the transmission diagram of Snowden et al. (1997), the e-folding column density for R45-band X-rays ($E_0 = 0.75$ keV) is also read as $N_H^0 = 3 \times 10^{21}$ H cm^{-2}. We adopt this value for the R45 band (0.75 keV). However, the *ROSAT* energy bands are rather broad, containing significantly higher and lower energies around the representative energies. In our simulation, therefore, we adopt three representative cross sections at the R12, R45, and R67 bands, which are 10, 1, and 0.1 times the value at 0.75 keV, respectively.

The neutral hydrogen layer is assumed to have a density distribution expressed by

$$n_H = n_0 \exp(-r/r_H - z/z_H) ,$$

where n_0 is the mean density in the solar vicinity and is taken to be $n_0 = 1$ H cm^{-3}, $r_H = 8$ kpc is the scale radius of the gas disk, and $z_H = 100$ pc is the scale height.

Figure 7*a* shows the calculated intrinsic intensity distribution, where no Galactic absorption is taken into account. Figure 7*b* is a result calculated for R45-band X-rays, which suffer from absorption by the Galactic atomic hydrogen layer. The observed absorption features near the Galactic plane are well reproduced by this model. The hypershells are observed as a set of double-horn features extending toward the Galactic poles, composing dumbbell-shaped ridges, and they mimic the observed X-ray spurs (NPS, NPS-West, SPS, and SPS-West). Figure 7*c* shows a case in which the hypershells are replaced by bipolar parabolic cones, which are open toward the polar axes, as illustrated in Figure 4*c*. The conical cylinder model appears, however, worse for reproducing the observed round shape

of the North Polar Spur in radio and X-rays. In both cases of hypershells and conical cylinders, the observed cylindrical spurs at lower latitudes in X-rays (Snowden et al. 1997) are well reproduced. The bulge component is also visible in the models, as the two enhanced regions above and below the Galactic center.

3.3.4. *X-Ray Sky with Spiral Arms*

Figure 8*b* (*middle panel*) shows results for a case in which the absorbing hydrogen gas is assumed to be condensed in logarithmic spiral arms of pitch angle 6° and the arm width is taken to be 1/5 of the arm separation, as illustrated in Figure 6. Hence, the peak hydrogen density in the local arm is about 5 H cm^{-3}. The hydrogen density distribution is expressed by

$$n_{\rm H} = \alpha n_0 \exp\left(-r/r_{\rm H} - z/z_{\rm H}\right) \cos^k\left(\theta - \eta \log r/r_0\right) .$$

Here, θ and η have the same meaning as in § 3.3.2. Since the tangential directions of the spiral arms are asymmetric around the Galactic center, the absorption feature near to the Galactic plane is also asymmetric.

In order to examine what the X-ray sky looks like in different energy bands, we have performed simulations for different values of the absorption coefficient. Figure 8 shows the calculated results for three different κ values: (*a*) 10 times the above value, (*b*) same as above, and (*c*) one tenth of the above. Figures 8*a*, 8*b*, and 8*c*, therefore, roughly correspond to X-ray views in the R12, R45, and R67 bands, respectively. In Figure 8, we compare the simulated results with the corresponding *ROSAT* images.

The R12-band model is characterized by a wide absorption lane along the Galactic plane, where X-rays from the Galactic plane and bulge are almost totally absorbed. The hypershells also suffer from strong absorption, while high-latitude parts are still visible as the northern and southern "polar caps," which are indeed observed in the *ROSAT* R12-band image. We also obtain a good reproduction of the observed *ROSAT* X-ray features in R45 and R67 bands, as discussed in the previous subsections.

3.4. *Summary of Comparisons between Models and Data*

We have revisited the hypershell model of radio and X-ray spurs around the Galactic center, and simulated the all-sky views of radio and X-ray emissions. The model can mimic the observed all-sky views fairly well in radio (Haslam et al. 1982) and *ROSAT* X-rays (Snowden et al. 1997), as shown in Figures 5, 7, and 8. The simulation could reproduce the following characteristic properties for the galactic spurs:

1. The major spurs in the whole sky are found around the Galactic center at $330° < l < 30°$ (NPS, NPS-West, SPS, and SPS-West).
2. These four spurs are located apparently symmetric with respect to the rotation axis of the Galaxy as well as to the Galactic plane.
3. Southern X-ray spurs exhibit cylindrical appearance.
4. X-ray spurs in R45 (0.75 keV) and R67 (1.5 keV) bands exhibit a sharp absorption lane along the Galactic plane.
5. R12-band (0.25 keV) spurs comprise northern and southern polar caps at high latitudes, $b > \sim 30°$–$40°$, while lower latitude emission is hardly visible because of a broad and strong absorption lane in the local Galactic plane.
6. An X-ray bulge is visible above and below the Galactic center in R45 and R67 bands.
7. Besides the BHS-related spurs, a greater number of radio continuum spurs are observed in the tangential directions of the inner and local spiral arms, with the most prominent spiral-arm spurs emerging at $l \sim 80°$ and $l \sim 260°$ corresponding to the local arm.

4. DISCUSSION

4.1. *Starburst Origin of Bipolar Hypershells*

4.1.1. *Timescale and Energetics*

In our model, the energy injection at the Galactic center has been assumed to be impulsive, and the shock is strong enough to create a well-defined shell structure. The timescale of the explosive event at the Galactic center is assumed to be sufficiently shorter than the expanding timescale of the hypershell. Since the expanding timescale is of the order of $t \sim r/v \sim 10^7$ yr for $r \sim$ several kpc and $v \sim 300$ km s^{-1}, the explosion timescale should be shorter than a few million years. The required total energy given to the interstellar gas is of the order of 10^{55}–10^{56} ergs in order to heat the gas up to $\sim 10^7$ K at the BHS front. Such impulsiveness and robustness of the energy release can be explained if the Galactic center experienced a starburst about 15 million years ago, lasting for a few million years or less, during which $\sim 10^5$ Type II supernovae exploded. If this starburst model is correct, the *ROSAT* all-sky data can be used to directly date and measure the energy of the recent starburst in our Galaxy.

4.1.2. *Hypershell's Neck in the Disk and the* 2.4 kpc *Expanding Ring*

By an MHD wave approximation of a blast wave from the Galactic center it was shown that a significant fraction of low-latitude front focuses on the Galactic plane, with the gas-flow paths being diffracted because of velocity gradient, which leads to an expanding gaseous ring in the disk (Sofue 1977). The tangential directions of this expanding ring in the present model, which coincide with the BHS dumbbell's neck, are at $l \sim \pm 20°$. In fact, the root of the observed radio NPS crosses the Galactic plane at $l \sim \pm 20°$ (Sofue & Reich 1979). It is interesting to point out that there is an expanding feature in the H I line emission in coincidence with this tangential direction of the hypershell, known as the "3 kpc (2.4 kpc) expanding ring" of H I gas (Oort 1977). Since the expanding velocity of the hypershell in the disk region is significantly decelerated, the ring will not be heated up to emit X-rays, and, therefore, the ring may not be detectable in X-rays at this low latitude.

The Milky Way is also known to have another gaseous ring in the disk, the "4 kpc molecular ring," with high-density concentration of molecular and H I gases. Although there is a suggestion about its origin as due to a resonance in a barred potential (Nakai 1992), it may also be possible to explain such a larger radius ring by focusing on an older expanding blast wave induced by an earlier starburst recurring in the Galactic center.

4.2. *Alternative Interpretations*

4.2.1. *Alternative Impulsive Energy Injections at the Galactic Center*

We may consider some alternative mechanisms for causing an impulsive energy release in the Galactic center region. One possibility is a single gigantic explosion at the

Galactic nucleus (Oort 1977), possibly caused by an infall of a star or its debris into the central massive black hole (Genzel et al. 1997; Ghez et al. 1998). A stellar wind–driven Galactic wind (Heckman et al. 1990) could also produce a shell structure, as observed with *ROSAT* for NGC 253 (Pietsch et al. 2000). However, if the wind is steady and longer lived than 15 million years, the flow would already have become open cone shaped, which does not appear to fit the observations. Another possible mechanism is a "meteorite-like impact" by infalling gas clouds from intergalactic space onto the Galactic gas disk, such as debris of the Magellanic Clouds after three-body dynamical interaction of the galaxies and the gas clouds. If several giant molecular clouds hit the gas disk at about the escaping velocity, ~ 400 km s^{-1}, and the kinetic energy is converted into heat, the impact will be equivalent to an explosion of energy of $\sim 10^{55}$ ergs.

Since the cooling time of the hypershell, which is of the order of 10^9 yr, is much longer than the expansion timescale, any of these mechanisms will result in similar shocked shells in the halo, if the total input energy is approximately the same.

4.2.2. *On the Local-Shell Hypothesis*

Although we have proposed a unified model to explain the galactic spurs in terms of a single event at the Galactic center, we cannot exclude the possibility that local objects such as nearby supernova remnants are superposed (Snowden et al. 1997). If we stand on the local-shell model, the sharp absorption lane along the Galactic plane in R45 and R67 bands must be explained by an intrinsic depression of intensity below $l \sim 10°$–$20°$. We have in fact simulated intensity distributions in soft X-ray bands as expected from a local uniform shell of diameter 300 pc at a distance of 200 pc embedded in a hydrogen layer of a scale height 100 pc and local density 1 H cm^{-3}. In R45 and R67 bands, no sharp absorption feature at $l < 10°$–$20°$ was obtained by the simulation because of the negligible extinction for its proximity. The absorption feature can be reproduced only if the shell is not a unique emission source, but it is superposed by a more distant emission such as from the Galactic bulge (Snowden et al. 1997). In R12 band, the local-shell model could mimic the observation, similarly to the hypershell model, because the distance does not affect the simulated results, since the absorption feature is produced very locally. Regardless of its distance, half the shell at high latitudes is visible in R12 band, while the lower half at $b < \sim 30°$ is absorbed by the local hydrogen layer.

A traditional idea for explaining the NPS is the local supernova hypothesis, which attributes the spur to a nearby shell of supernova remnant(s) of the largest diameter in the Galaxy, called Loop I (e.g., Berkhuijsen et al. 1971; Egger & Aschenbach 1995). The shell is the oldest supernovae remnant, and, therefore, the probability of detecting similar objects, if any exist in the Galaxy, is much higher than that of finding usual supernova remnants, almost two hundred of which are already discovered. Since the NPS is sufficiently bright in synchrotron radio emission, with the typical brightness being ~ 50 K at 408 MHz, and is apparently very large, such shells should have been easily detected if they existed anywhere in the Galaxy. In this sense, the NPS is a very unique (peculiar) object if we stand on the local supernova hypothesis. Note that Loops II and III, whose brightness temperatures are at most about 4 K at 408 MHz, are an order of magnitude less luminous than NPS. Note also that the major parts of Loops II and III can be explained by local arm spurs in the present model (Fig. 5; see also Sofue 1976).

4.3. *Implications of the BHS Model as a Probe of Halo and Intergalactic Gasdynamics*

4.3.1. *Halo-Intergalactic Interface*

If the bipolar hypershell model applies, the all-sky *ROSAT* X-ray and radio data can be used not only to measure the starburst, but also to probe the physics such as the density distribution and magnetic fields in the Galactic halo as well as those in the interface from the halo to intergalactic space. The morphology of the hypershell is sensitive to the density distribution in the halo, and particularly, the shell shape in the uppermost part manifests the halo-intergalactic density structure (Sofue 1984). If the intergalactic gas density is very low, the shell will become more open and conical, while if it is higher, the shell becomes more compact and round. The shell morphology, and therefore the density structure, is also dependent on the expanding velocity, which is directly related to the gaseous temperature inferred from soft X-ray spectra. More detailed hydrodynamical simulations with quantitative and morphological fitting to the *ROSAT* data would provide us with much advanced knowledge about the Galactic halo and intergalactic space in the Local Group.

4.3.2. *Asymmetry of the Hypershell*

The observed NPS and its southern counterspurs are asymmetric in morphology and intensities with respect to the Galactic plane as well as to the rotation axis of the Galaxy. Such asymmetry can be attributed to anisotropy in the halo and intergalactic space. Intergalactic wind, or equivalently, motion of the Galaxy in the Local Group, may also cause an asymmetry of the hypershell. Hence, the morphological appearance of the hypershell may be also used to probe the anisotropy and winds in the halo and intergalactic space.

We have not taken into account the local fluctuation of hydrogen gas and molecular clouds, which also cause asymmetry in the X-ray absorption appearance. In fact, the galactic layer is full of clouds, H I spurs, shells, and holes (Hartmann & Burton 1997). The Hydra spur of dense H I gas is a tilted spur emanating from the Galactic disk at $l \sim 20°$ toward $(l, b) \sim (0°, 30°)$, crossing the NPS root nearly perpendicularly, which would affect the absorption feature of the NPS. A more sophisticated modeling of the X-ray views and detailed comparison with the *ROSAT* survey is a subject for future simulations.

4.4. *Implications of the BHS Model for Large-Scale Structure in Nearby Galaxies*

As described in § 3.1, many spiral galaxies exhibit similar hypershells in their halos (Sofue 1984): NGC 253's dumbbell-shaped shells (Vogler & Pietsch 1999a; Pietsch et al. 2000); NGC 3079's shells in radio continuum, Hα, and X-rays (Duric et al. 1983; Pietsch, Trinchieri, & Vogler 1998; Veilleux et al. 1994); M82's bipolar cylindrical jets (Nakai et al. 1987). NGC 4258's anomalous arms could also be due to some out-of-plane partial shells (van Albada & van der Hulst 1982; Vogler & Pietsch 1999b). We stress that these out-of-plane features, including our hypershell in the

Milky Way, require a similar amount of total energy of the order of 10^{55}–10^{56}, or 10^4–10^5 Type II supernovae. This fact suggests that the BHS starburst model would be more general to model the extragalactic cases. Simulations of *ROSAT* X-ray features in these objects based on our model, which is in preparation, would provide us with a clue to date and measure the responsible explosive events at their centers, such as their starburst history as well as information about the gasdynamics in their halo-intergalactic interface. Such simulations would also give a clue to compare the halo-intergalactic gas physics and starbursts in external galaxies with those in our Milky Way.

5. SUMMARY

We have revisited the BHS model of the North Polar Spur and related Galactic structures based on the 408 MHz radio continuum and *ROSAT* all-sky soft X-ray data. We have shown that the NPS and its western and southern counterspurs draw a giant dumbbell shape on the sky, necked at the Galactic plane. The morphology and soft X-ray intensities of the spurs can be interpreted as due to a shock front originating from a starburst at the Galactic center some 15 million years ago with a total energy of the order of $\sim 10^{56}$ ergs or 10^5 Type II supernovae.

We have simulated radio continuum and soft X-ray skies based on the BHS Galactic center starburst model. Simulated all-sky distributions of radio continuum intensities can well reproduce the radio NPS and related spurs, as well as many other radio spurs in the tangential directions of spiral arms. Simulated soft X-ray maps in 0.75 and 1.5 keV bands can reproduce the *ROSAT* X-ray NPS and its western and southern counterspurs, as well as the absorption layer along the Galactic plane. The observed R12 band polar-cap features are also well reproduced in our model.

If the present BHS model for the spurs is correct, we may be able to use the *ROSAT* all-sky maps to probe the gasdynamics in the halo-intergalactic interface. We may also be able to directly date and measure the energy of a recent Galactic center starburst in the Milky Way, which can also be compared with similar BHS phenomena in nearby starburst galaxies.

The author would like to thank the *ROSAT* experiment staff for making the FITS formatted data of the X-ray survey available via an Internet link to "SkyView" operated by NASA. The author is indebted to the anonymous referee for the invaluable comments and suggestions, with which the paper has been very much improved.

REFERENCES

Berkhuijsen, E., Haslam, C., & Salter, C. 1971, A&A, 14, 252
Duric, N., Seaquist, E. R., Crane, P. C., Bignell, R. C., & Davis, L. E. 1983, ApJ, 273, L11
Egger, R. 1993, Ph.D. thesis, Univ. Munich
Egger, R. J., & Aschenbach, B. 1995, A&A, 294, L25
Genzel, R., Eckart, A., Ott, T., & Eisenhauer, F. 1997, MNRAS, 291, 219
Ghez, A., Morris, M., Klein, B. L., & Becklin, E. E. 1998, ApJ, 509, 678
Hartmann, D., & Burton, W. B. 1997, in Atlas of Galactic Neutral Hydrogen (Cambridge: Cambridge Univ. Press), 53
Haslam, C. G. T., Salter, C. J., Stoffel, H., & Wilson, W. E. 1982, A&AS, 47, 1
Heckman, T. M., Armus, L., & Miley, G. K. 1990, ApJS, 74, 833
Laumbach, D. D., & Probstein, R. F. 1969, J. Fluid Mech., 35, 53
McCammon, D., Burrows, D. N., Sanders, W. T., & Kraushaar, W. L. 1983, ApJ, 269, 107
McCammon, D., & Sanders, W. T. 1990, ARA&A, 28, 657
Möllenhoff, C. 1976, A&A, 50, 105
Morrison, R., & McCammon, D. 1983, ApJ, 270, 119
Nakai, N. 1992, PASJ, 44, L27
Nakai, N., Hayashi, M., Handa, T., Sofue, Y., Hasegawa, T., & Sasaki, M. 1987, PASJ, 39, 685
Oort, J. H. 1977, ARA&A, 15, 259
Pietsch, W., Trinchieri, G., & Vogler, A. 1998, A&A, 340, 351
Pietsch, W., Vogler, A., Klein, U., & Zinnecker, H. 2000, A&A, in press
Ryter, Ch. E. 1996, Ap&SS, 236, 285
Sakashita, S. 1971, Ap&SS, 14, 431
Snowden, S. L., et al. 1997, ApJ, 485, 125
Sofue, Y. 1976, A&A, 48, 1
———. 1977, A&A, 60, 327
———. 1984, PASJ, 36, 539
———. 1993, PASP, 105, 308
———. 1994, ApJ, 431, L91
Sofue, Y., & Reich, W. 1979, A&AS, 38, 251
Tomisaka, K., & Ikeuchi, S. 1988, ApJ, 330, 695
Uchida, Y., Shibata, K., & Sofue, Y. 1985, Nature, 317, 699
van Albada, G. D., & van der Hulst, J. M. 1982, A&A, 115, 263
Veilleux, S., Cecil, G., Bland-Hawthorn, J., Tully, R. B., Fillippenko, A. V., & Sargent, W. L. W. 1994, ApJ, 433, 48
Vogler, A., & Pietsch, W. 1999a, A&A, 342, 101
———. 1999b, A&A, 352, 64